# Beneath the Perforators: Unravelling Fascia Lata Intrinsic Vascular Architecture using microfocus X-ray computed tomography

**SHORT RUNNING TITLE:** Intrinsic Vascularization of Fascia Lata

Julie Manon, PT, MD, PhD[1-3,5*], Eléonore Gillerot, CE[4], Frédéric Delandmeeter, PT[5], Lucien Van den Broeck[5], Pierre Schneidewind[4,5], Emmanuel Coche, MD, PhD[6], Grzegorz Pyka, CE, PhD[4,7], Olivier Cornu, MD, PhD[1-3], Catherine Behets, MD, PhD[5], Greet Kerckhofs, CE, PhD[4,7], Benoît Lengelé, MD, PhD, FRCS[5,8]

[1]*Université Catholique de Louvain (UCLouvain) – Institut de Recherche Expérimentale et Clinique (IREC), Neuromusculoskeletal Lab (NMSK), Avenue Emmanuel Mounier 53 - B1.53.07, 1200 Brussels, Belgium*

[2]*Cliniques universitaires Saint-Luc, Department of Orthopedic and Trauma Surgery, 1200 Brussels, Belgium*

[3]*Cliniques universitaires Saint-Luc, Department of Cell and Tissue Therapy, 1200 Brussels, Belgium*

[4] *UCLouvain – IREC, ContrasTTeam, Avenue Emmanuel Mounier 52 - B1.52.00, 1200 Brussels, Belgium*

[5]*UCLouvain - IREC, Morphology lab (MORF), Avenue Emmanuel Mounier 52 - B1.52.04, 1200 Brussels, Belgium*

[6]*Cliniques Universitaires Saint-Luc, Department of Radiology, 1200 Brussels, Belgium*

[7]*UCLouvain – Institute of Mechanics, Materials, and Civil Engineering (IMMC), Mechatronic, Electrical Energy and Dynamic Systems (MEED), 1348 Louvain-la-Neuve, Belgium*

[8]*Cliniques universitaires Saint-Luc, Department of Plastic and reconstructive Surgery, 1200 Brussels, Belgium*

***Corresponding author:**

Julie MANON, PT, MD, PhD

*Institut de Recherche Expérimentale et Clinique (IREC), Neuromusculoskeletal Lab (NMSK), Avenue Emmanuel Mounier 52 - B1.52.04, 1200 Brussels, Belgium*

*Cliniques universitaires Saint-Luc, Department of Orthopedic and Trauma Surgery, Avenue Hippocrate 10, 1200 Brussels, Belgium*

julie.manon@uclouvain.be, +32 (0) 495/61.15.64 or +33 (0) 665670985

ORCID number: 0000-0002-2558-8723

# ABSTRACT

## Introduction

The fascia lata (FL), a dense connective tissue enveloping the deep structures of the thigh, has served as an avascular scaffold for decades in reconstructive surgeries, but never as a standalone vascularized flap, because its vasculature is only described by perforating vessels coming from the lateral circumflex femoral artery without specific intrinsic vasculature. However, the demand for vascularized tissue replacements requires a thorough understanding of this inherent vascularization. Based on the anterolateral thigh (ALT) flap knowledge, this study explores the detailed quantitative vascular architecture of the FL, from the perspective of using it as a standalone vascularized flap.

## Material & Methods

High-resolution microfocus X-ray computed tomography (microCT) of Angiofil-latex injected flaps allowed us to study the specific fascial distribution of perforators. Dissections of 11 fresh-frozen lower limbs identified the main perforating arterioles. The intrinsic vascular network within the FL tissue was then analyzed using microCT.

## Results

The study confirmed an average of 2.5±0.5 main perforating trunks giving rise to 5.6±2.9 perforating arterioles per thigh. Notably, microCT revealed a distinct intrinsic vascular network within the FL tissue, with tiny arterioles of 55.39±28.47µm radius and a volumetric density of 33,347,960±23,243,879µm³/mm². This intrinsic vasculature exhibited a high density of bifurcations (branching nodes=1.36±2.26/mm²), demonstrating its potential use as a vascularized flap.

## Discussion

This study unveils the intrinsic vascularization of the FL, supporting its utility as a mega-thin vascularized flap in reconstructive surgery. Based on this vascular carrier, these findings also open new applications for tissue engineering and personalized medicine, toward an improvement of surgical outcomes and patient recovery.

**Keywords**

Fascia lata, Intrinsic vascularization, Anterolateral thigh flap, Perforators, Angiofil-latex vascular injection, Microfocus X-ray computed tomography, Very-thin flap

## 1. INTRODUCTION

The fascia lata (FL) is a dense connective tissue enveloping the thigh, with a lateral thickening known as the iliotibial tract (ITT). Composed of collagen fibers (Manon et al., 2022) with a specific organization (Manon et al., 2024c), this tissue has been used for several decades in reconstructive surgeries as a replacement tissue or avascular mesh (Stecco et al., 2013). Typically decellularized and stored in tissue banks (Fawzi-Grancher et al., 2009; van Steenberghe et al., 2017), the FL is used in various procedures, such as duraplasty (Finn et al., 2011), colpopexy (Bock et al., 2021), abdominal wall repair (Disa et al., 1998; Stecco et al., 2013; Song et al., 2018), maxillofacial reconstruction (Alemán and Martínez, 2012; Karaaltin et al., 2012), or ligamentoplasties (Ferretti et al., 2017; Matthewson et al., 2020). However, optimal tissue regeneration in transplantation requires an effective vasculature, crucial for nutrient supply and cell survival. Understanding the FL intricate vascular network is thus pivotal for enhancing its potential in regenerative medicine.

The renowned anterolateral thigh (ALT) flap garnered interest due to its significant vascular properties. Described forty years ago (Song et al., 1984), it is based on perforating vessels arising from the descending branch (DB) of the lateral circumflex femoral artery (LCFA), and offers a reliable long vascular pedicle despite several branching variations. The ALT flap is valued for its ease of harvesting, adaptable shape and size, large vessel diameter (2.0 to 2.5mm (Song et al., 1984; Shieh et al., 2000)), moderate thickness, and ability to incorporate sensitive functions. It also boasts minimal donor-site morbidity with usual primary closure (Song et al., 1984; Shieh et al., 2000; Yu, 2004; Sananpanich et al., 2008; Lakhiani et al., 2012; Saint-Cyr et al., 2012; Fox et al., 2014; Smith et al., 2017; Sapino et al., 2019; Buergin et al., 2022). Widely used in reconstructive surgery, the ALT flap is usually raised as a thin or ultra-thin skin flap. Including the FL, a composite flap has been also used for patellar or Achilles tendon reconstruction combining a skin paddle with

a fascial strip, and mimicking a tendon-like structure (Kuo et al., 2008; Song et al., 2013; Youn et al., 2015; Ehrl et al., 2019; Sapino et al., 2019; Imaizumi and Toyota, 2022; Liang Yii et al., 2022).

Although previous studies have extensively characterized ALT vascularization, specifically its subdermal and suprafascial vascular plexuses (Song et al., 1984; Shieh et al., 2000; Janik et al., 2020), the intrinsic vascularization within the FL itself remains largely unexplored. Unveiling this network could open the possibility of using a fascial-only vascularized flap.

Alongside reviewing the vascular distribution from the LCFA to the thigh integuments, the primary objective is to uncover the intrinsic vascularization within the FL. The clinical CT scan can reach a maximal resolution of 0.3mm (Manon et al., 2024b) that cannot highlight microvasculature inside the FL. Supposing that FL intrinsic vessels would be thinner than the perforator, an emerging technology was used to investigate deeper details. The microfocus X-ray computed tomography (microCT) allowed a high-resolution 3D study of the specimens until the microscopic level (Leyssens et al., 2021), without tissue damage like caused by histology or microstructure changes caused by dissection. This microscopic exploration, combined with advanced injection techniques (Angiofil- latex (Manon et al., 2024b)), aims to reveal previously unseen micro-vessels within the FL tissue, shedding light on its vascular intricacies.

## 2. MATERIAL & METHODS

### *2.1. Fascia lata (FL) procurement*

Fresh frozen lower limbs (N=16) were provided by the Human Anatomy Department of UCLouvain (IRB00008535, Brussels, Belgium) with approval from the local ethics committee (Ref 2021-

30AOU-356, approved on September 13, 2021). The study, divided into macroscopic and microscopic assessments, details specimen demographics for each part in Table 1.

### *2.2. Angiofil-latex injection*

All limbs underwent successful Angiofil-latex intravascular injection according to the previously described technique (Manon et al., 2024b). Briefly, they were thawed in a hip-down position, then rinsed with pre-heated (56°C) NaCl solution (0.9%) through the femoral artery (FA). Injection was performed through the LCFA under continuous manual pressure and involved a latex mixture (*Latex "LA", with 0.38% ammonia, 603, Finres, Belgium*) supplemented with a 1:5 volume of liposoluble iodine agent (*Angiofil, S500.0028, Fumedica AG, Switzerland*) (mixture 1:5 contrast agent: solvent, v/v), and red dye droplets (*Jesmonite, bright red pigment, 200g, Finres, Belgium*). Angiofil allowed vascular opacification for CT and microCT imaging, while latex facilitated solidification in a cold room (4°C) for 72h. After solidification, the vascular tree was fixed and preserved for subsequent analysis at any time in both imaging and/or dissection.

### *2.3. Lateral circumflex femoral artery (LCFA) vascular network distribution and perforators*

#### Computed tomography (CT)

The precise artery opacification permitted maximal resolution in clinical CT images (0.3mm) (Manon et al., 2024b). This technique evaluated the LCFA vascular network and its perforators (Saint-Cyr et al., 2008). Lower limbs (N=11) were imaged between injection and solidification time, using a Somatom Definition AS 128 scanner (*Siemens Healthineers, Erlangen, Germany*), in an ultra-high-definition mode (beam collimation=0.3mm, tube voltage=120kV, tube current=200–250mAs). Subsequent reconstructions using both hard and soft kernels (slice thickness=0.4mm) and volume rendering technique (Dappa et al., 2016; de Spiegeleire et al., 2019), were performed

with the SyngoVia tool in cinematic rendering mode. CT acquisitions and reconstructions were useful for 3D visualization and dissection planning.

#### Dissection

Following latex solidification, limbs were dissected according to previously reported protocols (Saint-Cyr et al., 2012; Lee et al., 2015; Manon et al., 2022, 2023). The skin incision followed the standard landmarks between the anterior superior iliac spine (ASIS) and the superolateral border of the patella. The DB of the LCFA was first identified distally between the vastus lateralis and the rectus femoris. The LCFA was dissected retrogradely, encompassing the DB and the transversal branch (TB) up to the injection catheter. Dissection continued anterogradely through the septum or the vastus lateralis until reaching the distal perforators. All the perforator pathways were carefully dissected between the LCFA and the FL to reveal the entire LCFA vascular network.

#### Data collection and analysis

The LCFA vascular network was macroscopically described using a combination of Yu's ABC system and Shieh's vascular classification (Yu, 2004; Lee et al., 2015). Yu's classification (Yu, 2004) identified three levels, *i.e.* at the midpoint between the ASIS and the patella (perforator B), and 5cm proximally (perforator A) or distally (perforator C) from this point. Shieh's classification (Lee et al., 2015) focused on perforator origin, number, location, and musculo- or septocutaneous characteristics of each pathway. When main perforator trunks gave rise to small perforating branches, they were documented. Qualitative data were expressed as frequency, *i.e.* number of events and percentage.

### *2.4. Intrinsic vascularization of the FL*

#### Dissection

Following latex solidification, dissection included a more medial (1cm) skin and fascial incision to flip and lift the entire fasciocutaneous ALT flap (N=5), preserving all perforating vessels (Saint-Cyr et al., 2012; Lee et al., 2015; Manon et al., 2024b). The incision proceeded vertically through the subcutaneous tissue until passing beneath the FL. The perforators were identified just under the FL and cut on their original side. The full-thickness flap was harvested, preserving all perforating arterioles (Fig. 1 – a), and was fixed in 4% formaldehyde (VWR, 9713.9010) for 4 days at room temperature. A thread in the antero-superior corner always provided a precise orientation of the tissue (Fig. 1 – Dark blue arrows).

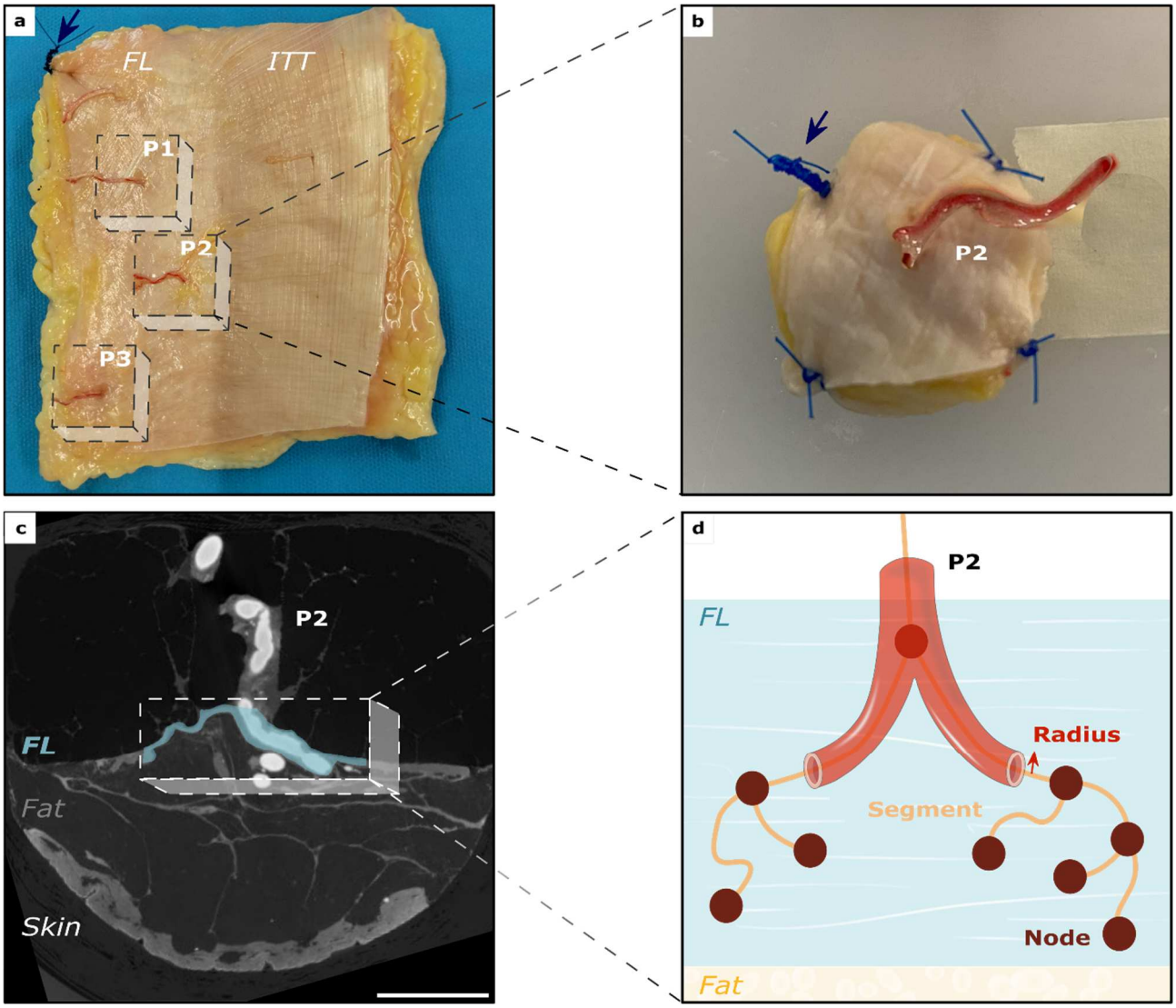

*Figure 1. Study design of the experiment. Harvesting of the full-thickness fasciocutaneous anterolateral thigh flap (N=5 donors), seen from its deep surface and divided into two parts, the fascia lata (FL) and the iliotibial tract (ITT) (a). Cubes of 2x2cm are harvested, centered on the perforating artery (P2 for example in this figure) (n=3 cubes x 3 donors=9) (b). Full-thickness cubes were imaged with microCT and extraction of subvolume containing only the FL tissue was highlighted in light blue (c), which directly permitted the quantification of the vasculature volume inside the FL (d). Autoskeleton module allowed to skeletonize the vascular network into segments and branching nodes that were quantified. Dark blue arrows: Orientation thread in the antero-superior corner. Note that the harvested samples are somewhat distorted by the fixation threads sutured at the four corners of the cube, which thus takes the form of a cushion. This artifact slightly alters the native parallelism between the anatomical planes of the deep fascia and skin surface, as well as the native disposition of vascular networks. White scale bar: 5mm.*

**Angiofil-latex enhanced microCT**

Angiofil-latex filled full flaps were first imaged with a Phoenix NanoTom M (*Baker Hughes Waygate*) (Table 2 – Low-resolution) to get an idea of the perforator distribution. The location of the perforating points through the fascia was recorded and classified as being in the ITT, in the anterior fascia, or at the junction between the two.

To increase the spatial resolution, three flaps (N=3 donors) were trimmed into full-thickness cubes with a surface area of 2x2cm centered on three perforators, meaning 1cm on either side (n=3 cubes x 3 donors=9) (Fig. 1 – b). The four corners of the cube surface were stitched from the fascia to the skin to avoid delamination of tissue components during the microCT. The cubes were mounted on polystyrene blocks with the perforators within a centered hole, wrapped in parafilm, and imaged with the Phoenix NanoTom M (Table 2 – High-resolution).

**Image processing and analysis**

The Angiofil-latex mixture contrasted the vascular network in white, enabling detailed intrafascial analyses using Avizo software (2022.1, ThermoFisher Scientific, France). Several processing tools were applied successively. First, the FL and the vascular tree were segmented using *semi-manual segmentation tools (brush and magic wand),* and the *Filter Sandbox* module thanks to their grey values. The sample 3D visualization was made using the *volume rendering* tool and allowed a qualitative and visual analysis of the intrinsic FL vascularization.

Subvolumes containing the FL thickness-only were extracted using a combination of *Extract Subvolume* and *Arithmetic* modules (Fig. 1 – c), and structural data were obtained. The volume of the vasculature inside the FL was quantified using the *Volume fraction* tool, normalized by the subvolume surface, and expressed as mean ± standard deviation (SD) of three samples for the three donors. The normalized volume of the main perforating arteriole was manually calculated based on diameter and fascial thickness and subtracted from the total normalized vascular volume to estimate the effective FL vascularization volume. A ratio of vascular subvolume to tissular subvolume was computed and expressed as mean percentage ± SD. The number of vascular segments, branching nodes, and arteriole radius were computed from the *Autoskeleton* module (Fig. 1 – d, smoothing coefficient 0.5 (smooth) – 0.25 (attach to the data), number of iterations 10). A vascular segment is defined as a continuous curvilinear segment between two nodes. A node is determined by the vascular ramification into a minimum of two smaller vessels. The variables of segments and branching nodes were normalized by respective subvolume surface, averaged, and expressed as mean ± SD.

## 3. RESULTS

### *3.1. Distribution of the LCFA vascular network and its perforators*

Among the 11 dissected full thighs, 28 main perforators were identified, averaging 2.5 ± 0.5 main perforator trunks per LCFA territory. The DB and the TB yielded 1.1 ± 0.5 and 1.5 ± 0.8 perforators, respectively. The perforator distribution and pattern were described in Table 3, following Yu's classification (Yu, 2004), with the number of limbs that exhibit at least one perforator of each level. Perforators A and B were mostly septocutaneous while perforators C were always musculocutaneous. Each LCFA territory (100%) featured at least one perforator B, the most prevalent (35.7%).

Combining Yu's system with Shieh's classification (Additional Table A), no thigh had only one perforator in this study. The most common pattern involved triple perforators from both the DB and the TB (55%).

Additionally, 62 small perforating branches emerged from main perforator trunks to cross the FL, averaging 5.6 ± 2.9 perforating arterioles per limb.

### *3.2. Intrinsic vascularization of the FL*

Among five entirely raised flaps, 28 perforating arterioles were contrasted, *i.e.* 5.6 ± 1.5 perforating arterioles per ALT flap, consistent with the results summarized in Additional Table A. The fascial perforating point of arterioles was found twice in the ITT (2/28 – 7.1%), eight times in the junction (8/28 – 28.6%), and most frequently in the anterior thigh fascia (18/28 – 64.3%). The mean diameter of these arterioles was 0.61 ± 0.38mm.

To the naked eye, the qualitative exploration of the entire flaps suggested distinct types of perforating arterioles, some of them running along the fascia surface with/without ramifications that could vascularize the FL by diffusion (Fig. 2 – a). However, in most cases, no well-defined

intrinsic vascularization was macroscopically apparent (Fig. 2 – b). Further examinations revealed that some perforators sent branches to the adipose side of the FL (Fig. 2 – c & Video 1), although this vascularization was not easily observable through the FL opacity. Another difficulty is the discrimination to be made between arterioles running within the fascia or just lying down the FL. Therefore, microCT imaging was performed.

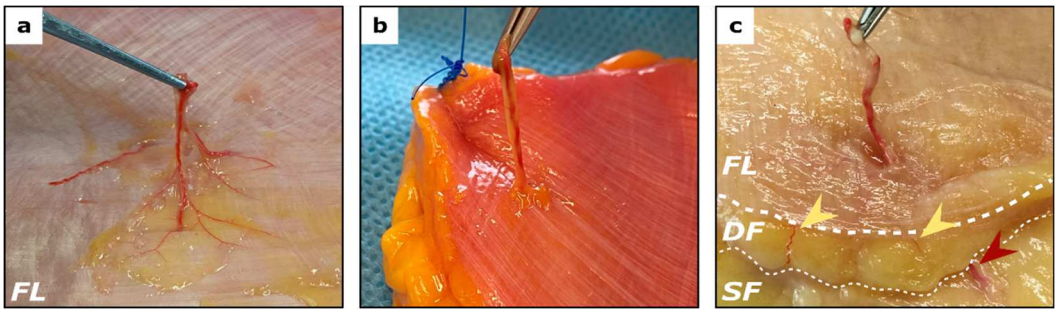


*Figure 2. Macroscopic visualization of perforating arterioles: ramified perforator in the subfascial gliding plane (a), isolated perforator (b), and perforating vessel that branches in/after the fascia lata (FL) (c). DF: deep fat, SF: superficial fat. Yellow arrowheads show ramified branches, running along the FL. Red arrowhead marks the continuity of the main perforating arteriole. The thin dotted line runs along the superficial fascia.*

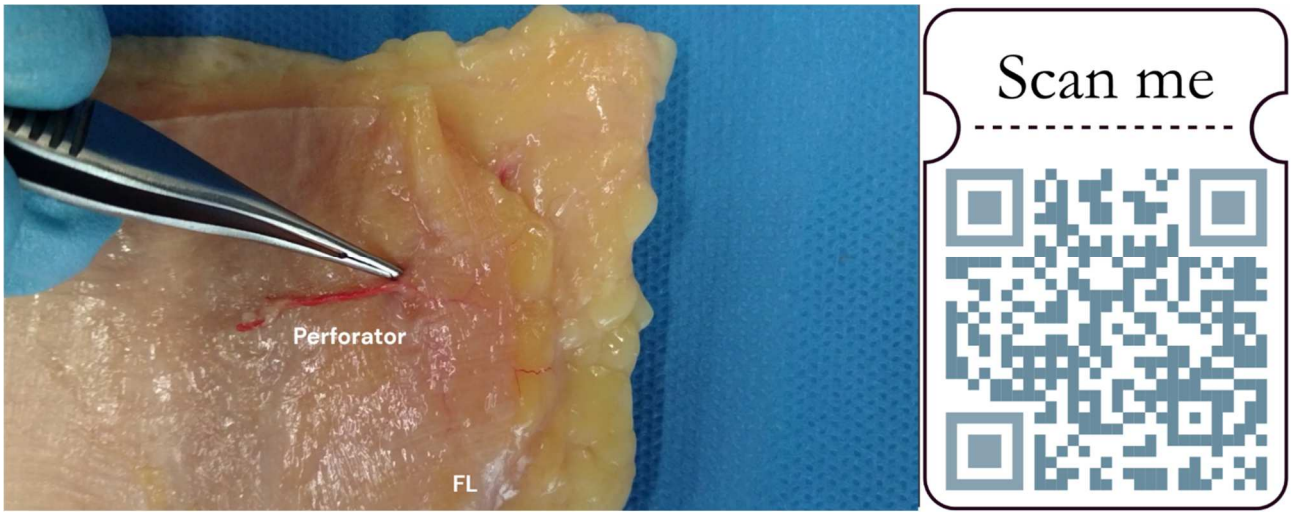

*Video 1. Perforating arteriole that ramifies in/after the fascia lata in the intra- and suprafascial plexus, respectively, before sending a connecting artery toward the subdermal area. FL: fascia lata, DF: deep fat, SF: superficial fat.*

*https://zenodo.org/records/11060858?token=eyJhbGciOiJIUzUxMiJ9.eyJpZCI6ImYyODE1MWE3LTE4MTItNGQ2NC1iYTkyLTRjMDVjYzIwZTE0NSIsImRhdGEiOnt9LCJyYW5kb20iOiIxNjE5OGY0ZGU5MWUzZmZmYzU5ODU4NDQyNjJjNGMzZSJ9.Ui2PjWPIklbPMl4ma33-ck1-XZEVTP5QCx4Bf5PUk4bodhMFBYVAksaVPdqkr6apPK3OsB-w4XIyr54TUrLgRw*

MicroCT data showed contrasted arterioles within ALT flaps (Fig. 3 – a). However, distinguishing fascial intrinsic vessels from extrinsic ones was challenging at low-resolution. MicroCT analysis of cubes of 2 cm side revealed small Angiofil-latex enhanced arterioles within the FL itself emerging from the main perforator and running through the FL, providing its vascularization (Fig. 3 – b). 3D renderings confirmed this observation, with the intrinsic fascial vascularization highlighted in yellow (Fig. 3 – c), obviously distinct from extrinsic vessels colored in red. The 3D view highlighted the arborescence of both intrinsic and extrinsic vasculature, with centrifugal arterioles spreading towards the skin and giving rise to four different networks identified as subfascial, intrafascial, suprafascial, and subdermal plexuses. These plexuses are arranged parallel to the FL and the skin, with orthogonal arterioles acting as connecting vessels. The intrinsic yellow arterioles and suprafascial red arterioles exhibit a similar meshwork organization but in two juxtaposed parallel planes, both featuring arborescent patterns and branching ramifications with curved paths.

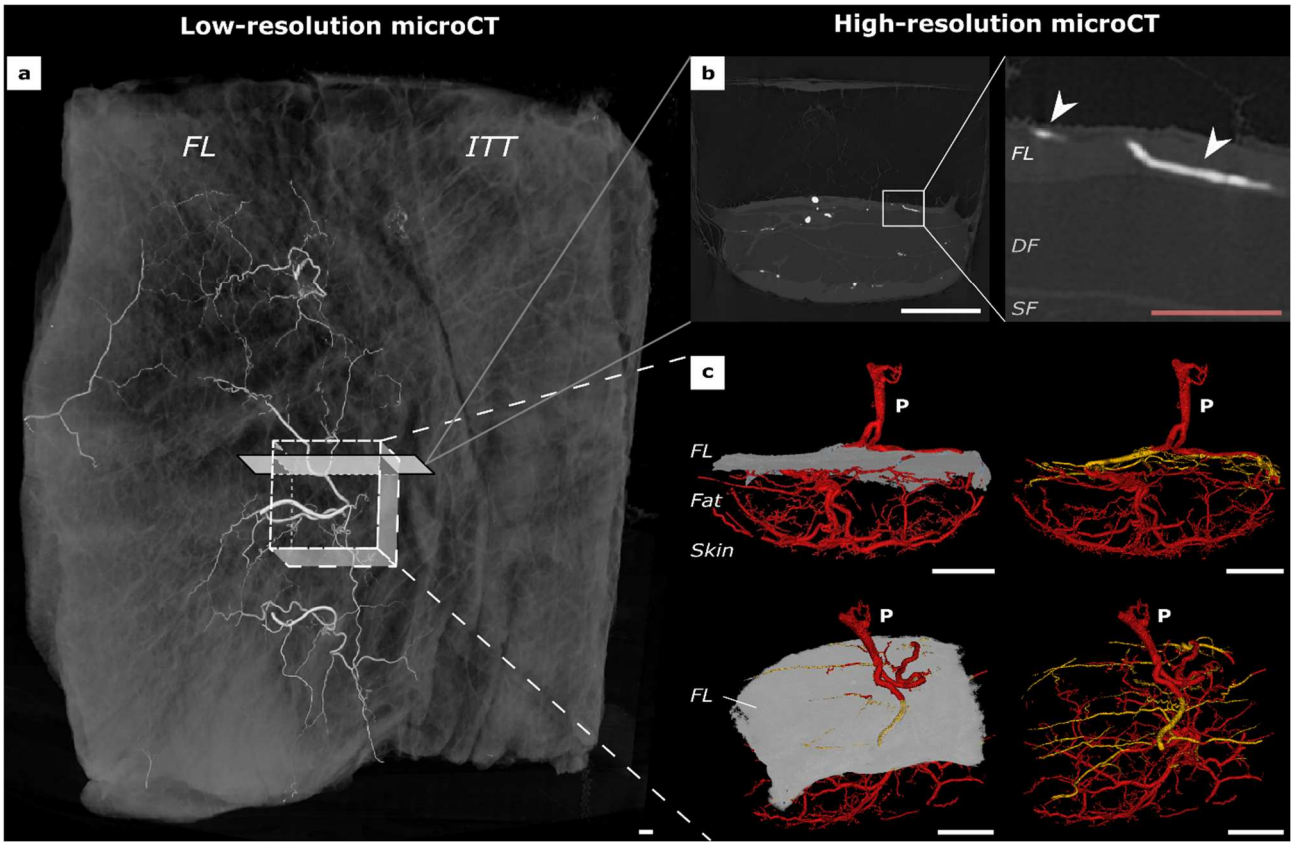


*Figure 3. Low-resolution Angiofil-latex enhanced microCT of the whole ALT flap divided into two parts, the fascia lata (FL) and the iliotibial tract (ITT) (a). High-resolution Angiofil-latex enhanced microCT cross-section of a full-thickness cube (b) and 3D renderings (c) highlighting the extrinsic vascularization (red) and the intrinsic vascularization (yellow), emerging from a perforating arteriole (P), before and after removing the segmented FL in grey. DF: deep fat, SF: superficial fat. White arrowheads: intrinsic vessels. White scale bars: 5mm, pink scale bar: 1mm.*

Quantitatively, the total normalized volume of intrinsic arterioles within the FL averaged 35,622,356 ± 23,416,866µm³/mm² of FL surface. Considering the volume of the perforating arteriole at 2,274,396 ± 2,020,080µm³/mm², the effective volume of arterioles inherently vascularizing the FL was 33,347,960 ± 23,243,879µm³/mm² of tissue surface. The ratio between

vascular subvolume and tissular FL subvolume was 1.05% ± 0.34. The mean arteriole radius inside the FL was 55.39 ± 28.47µm.

The average number of intrinsic vascular segments was 2.55 ± 4.16/mm², with 1.36 ± 2.26/mm² branching nodes, indicating the arborescence and ramifications.

## 4. DISCUSSION

Supported by the advantages of both Angiofil-Latex intravascular injection (Manon et al., 2024b) and high-resolution microCT (Leyssens et al., 2021), this study confirmed the macroscopic distribution of LCFA perforators and importantly unveiled the existence of an intrinsic vascular network within the FL.

**LCFA vascular network**

Like the LCFA origin variability (Tomaszewski et al., 2017), the arborescence of LCFA perforators has been previously studied. Predominant perforators were originally described in a circle of 3cm radius around the midpoint between the ASIS and the patella (Xu et al., 1988; Yu, 2004; Saint-Cyr et al., 2012). The variable anatomy in route (septocutaneous or musculocutaneous (Song et al., 1984; Xu et al., 1988; Shieh et al., 2000; Sananpanich et al., 2008)), origin (DB or TB (Yu, 2004; Lee et al., 2015)), orientation (horizontal or vertical (Shieh et al., 2000; Yu, 2004)) or level (Yu, 2004; Lin et al., 2010; Lakhiani et al., 2012; Lee et al., 2015) was however confusing (Koshima et al., 1989; Shieh et al., 2000; Lee et al., 2015; Tomaszewski et al., 2017). Several classifications followed one another with no strict consensus. In this study, Yu's and Shieh's systems allowed us to classify perforators depending on their height and origin and to detail their characteristics comprehensively.

On average 2.5 ± 0.5 main perforating trunks and 5.6 ± 2.9 perforating arterioles per LCFA territory were found, which corresponds to the literature data (1.6 to 3.2 perforators). Cadaver studies always counted more perforators (mean 2.7) than clinical ones (mean 2.1) (Yu, 2004; Lakhiani et al., 2012; Smith et al., 2017; Janik et al., 2020). Angiofil-latex injection enhanced perforator visualization and dissection, in opposition to surgical observations that concentrate on the main vascular pedicle and may lower consideration for secondary perforators (Sananpanich et al., 2008). The ALT is a reliable flap with at least one perforator in 98% of cases (Smith et al., 2017), but still, clinical studies found no perforator in 5.4% compared to 0% of cases in cadaver studies.

Patterns of perforators observed in this study included at least two perforators, and a predominance of triple perforators from both the TB and DB, differing from other studies (Yu, 2004; Lee et al., 2015). Data should be considered with caution given the small sample size. More extensive studies (N>70) and meta-analyses deserve greater confidence when describing a single predominant origin (57 to 100%) from the DB (Yu, 2004; Lakhiani et al., 2012; Lee et al., 2015; Smith et al., 2017).

More than 80% of the limbs exhibited at least one perforator from each level of Yu's classification. The musculocutaneous pattern was common (Kimata et al., 1998; Shieh et al., 2000; Yu, 2004; Sananpanich et al., 2008; Lakhiani et al., 2012; Lee et al., 2015; Smith et al., 2017), with perforator B being the most prevalent (85.6 to 100% in a circle of 5 to 6cm around the midpoint (Lakhiani et al., 2012)). The most distal level, the most musculocutaneous pathways were found. This simple classification is particularly useful to precisely guide the surgeon's decision. If needed or if perforator B is absent, both other perforators can help. Perforator C is usually thinner and most frequently musculocutaneous while perforator A has a larger diameter but might shorten the pedicle length and increase the fatty thickness (Yu, 2004; Lee et al., 2015), especially in Western people (Yu, 2004; Lakhiani et al., 2012). For all these reasons, even if some authors did not

recommend preoperative imaging (Lin et al., 2010; Saint-Cyr et al., 2012), Doppler investigations and angiography, in case of a negative Doppler, can considerably impact surgical planning and reduce the risk of failure (Yu, 2004; Sananpanich et al., 2008; Smith et al., 2017; Janik et al., 2020).

Even though the ALT versatility is tremendous, its bulkiness makes it unsuitable for indications requiring a very-thin vascularized membrane. The main value of the macroscopic analysis is to confirm that the sample is representative of typical LCFA pedicle variations, thereby supporting the reliability of micro-level findings on arteriole branch distribution within perforasomes. The groundbreaking advance then lies in the second part of our study which explored the intrinsic FL vascularization. Notably, the intrinsic distal microvascular arrangement within the fascial and cutaneous layers remains independent of the proximal macrovascular variations.

**Intrinsic FL vascularization**

Macroscopically, during the dissection, most perforating arterioles (64.3%) were located in the anterior thigh fascia, with an average diameter of 0.61 ± 0.38mm, considered medium caliber (Yu, 2004; Smith et al., 2017).

Unlike the limitations in the resolution of clinical imaging, Angiofil-latex enhanced microCT provided microscopic insights into the FL intrinsic vascularization. A single perforating arteriole gave rise to branches of 55.39 ± 28.47µm radius within the fibrous tissue, equivalent to approximately 0.1mm diameter. Their ramifications ran inside the FL allowing blood supply for cell and tissue survival.

Quantitative evaluation showed an effective vascular volume within the FL and a dense network of bifurcations, though the dispersion of the volume data was important. The methodology, being highly reproducible due to systematic parameter replication and operator-independent computerized analysis, underscores the intra- and interpersonal variability among the specimens.

To our knowledge, a detailed exploration of FL intrinsic vascularization for a unique fascial vascularized flap has not been extensively studied. Two previous studies approached this concept differently, with one focusing on TB and ascending branch vascularization through histological 2D analysis (Tokumoto et al., 2016). However, the DB, known to send numerous arterioles to the FL (Yu, 2004; Lakhiani et al., 2012; Lee et al., 2015), was not specifically assessed since it was only retrogradely opacified by injection of the profunda femoris artery (PFA) and/or the superior lateral genicular artery, and showed no macroscopic intrinsic opacification. The second study injected methylene blue into the DB to explore FL vascularization macroscopically (Janik et al., 2020). However, the adherent adipose tissue was not removed to preserve the perifascial blood supply. Therefore, the discrimination between real intrinsic vascularization and vessels lying down the FL surface was impossible. The authors also mentioned the limited value of methylene blue injection and consequent clinical impact (Janik et al., 2020), and openly suggested additional exploration with more detailed techniques.

In contrast, our study strongly suggests that the FL has its own supplying network which is the key message. Additionally, perforating branches of the LCFA give rise to a subfascial and suprafascial network, before spreading their terminal branches in the subdermal plexus.

**Limits, perspectives & recommendations**

The sample size was small but able to demonstrate the FL intrinsic vascularization. Future studies on larger cohorts and varied arteriole locations are warranted. Exploring anastomotic networks within the FL could offer insights into potential single-pedicle FL-only flap creation.

This intravascular injection method specifically highlights arterioles. However, the entire process could be adapted to the venous network to assess venous return. Identifying the nature of vessels—whether arteries, veins, or lymphatic vessels—could also be achieved through

immunohistochemistry (Pirri et al., 2023), though this approach carries the drawback of potential histological damage to the tissue. Efforts to develop specific staining agents compatible with microCT are ongoing to address this limitation.

This study, conducted on an elderly population with potential involution of FL tissue and its vascularization, suggests that if these findings are significant in older individuals, they could be even more pronounced in younger individuals.

The FL has already been processed in tissue banks (van Steenberghe et al., 2017; Manon et al., 2023) with appropriate decellularization protocol to create an acellular, non-immunogenic biocompatible scaffold while preserving its extracellular matrix and skeleton (Manon et al., 2023; Vettese et al., 2024; Manon et al., 2024a). However, its avascular nature limits some uses, highlighting the importance of vascular supply. Considering ongoing advancements in tissue engineering, detailed micro-level vascular network studies are essential prerequisites for potential recellularization efforts (Buergin et al., 2022).

Pending improvements in regenerative medicine, this revelation of an FL intrinsic vascular network supports using an FL-free flap as an autologous graft acting as a vascular carrier for cells of interest promoting tissue regeneration. Prioritizing examination of the anterior thigh fascia, rich in perforating arterioles, is recommended. The choice of perforators should align with surgical needs, with a preference for a middle perforator when possible due to optimal pedicle caliber, length, intrinsic vascularization, and thinness.

As such, its utilization could cover a huge panel of reconstructive surgery. A mega-thin vascularized FL flap including sub-, intra-, and suprafascial plexuses could benefit various clinical reconstructive conditions such as tympanoplasty (May et al., 2022), several mucosal repairs, head and neck defect covering in the management of osteoradionecrosis (Sreenath et al., 2023), or

replacement of extensive loss of physiological membranes such as dura mater, pleura or peritoneum (Tokumoto et al., 2016; Janik et al., 2020). However, further clinical applications in reconstructive or regenerative surgery necessitate stronger evidence and a more detailed study of these vascular networks, supplied by the LCFA perforators, which is ongoing in our laboratory.

## 5. CONCLUSION

The combination of Angiofil-latex intravascular injection and high-resolution microCT imaging offers a promising method to unveil the unseen aspects of FL vascularization. This study uniquely details the intrinsic FL vascular network, paving the way for the development of FL-only free flaps.

## Acknowledgments

The authors declare no conflict of interest.

Figure 1 was partly generated using templates provided by Servier Medical Art (http://smart.servier.com/, downloaded on the 14th of July 2022), licensed under a Creative Commons Attribution 3.0 unported license (https://creativecommons.org/licenses/by/3.0/, accessed on the 14 July 2022).

The authors would like to deeply thank their devoted colleagues for their contribution to this work, including Audrey Lentini, Laurie Gallant, Julia Vettese, Robin Evrard, Xavier de Spiegeleire, Christine de Ville de Goyet, Nicolas Charles-Pirlot, Bernard Caelen, all plastic surgery residents (Cliniques universitaires Saint-Luc, Brussels, Belgium), all members of the institutional tissue bank (Cliniques universitaires Saint-Luc, Brussels, Belgium), Gaspary Fodjeu, Loïc Fonkoue, Michelle Cougnon, and Walter Hudders.

Additionally, the authors would explicitly thank the donors of the bodies used in this study, as well as their families.

This study was made possible thanks to the contributions from the Christian Delloye's Fund, part of Foundation Saint-Luc. Support was also provided by the F.S.R. Fund ("Fonds Spécial pour la Recherche," Belgium) and F.N.R.S. Aspirant Fund ("Fonds National de la Recherche Scientifique", Belgium) awarded to Dr. Julie MANON (Application ID 40004991, Belgium). Benoît Lengelé, Greet Kerckhofs, and Grzegorz Pyka acknowledge the support from an ARC grant (ARC 18/23-094) and the SBO project of the Research Foundation Flanders (FWO; grant S007219N), respectively. Avizo 2022.1 (Thermo Fisher Scientific, France) software acquisition was supported by the Fonds de la Recherche Scientifique (FNRS - EQP - Tomo4D-U.N069.20).

## Data Availability Statement

All data analyzed during the study are included in this published article/Additional Data. The complete original datasets generated during the current study are available from the corresponding author upon reasonable request.

## Author contributions

All authors agree to be accountable for the content of the work.

**Julie MANON:** Conceptualization, Methodology, Investigation, Formal analysis, Visualization, Writing – original draft

**Eléonore GILLEROT:** Software, Investigation, Formal analysis,

**Frédéric DELANDMEETER:** Investigation, Formal analysis,

**Lucien VAN DEN BROECK:** Investigation, Formal analysis,

**Pierre SCHNEIDEWIND:** Software, Investigation,

**Emmanuel COCHE:** Writing – Review & editing, Resources

**Grzegorz PYKA:** Methodology, Software,

**Olivier CORNU:** Methodology, Writing – Review & editing, Supervision, Funding acquisition

**Catherine BEHETS:** Writing – Review & editing, Resources, Supervision, Funding acquisition

**Greet KERCKHOFS:** Methodology, Software, Writing – Review & editing, Resources, Supervision

**Benoît LENGELÉ:** Conceptualization, Methodology, Formal analysis, Visualization, Writing – Review & editing, Resources, Supervision

REFERENCES

Alemán, R.M., Martínez, M.G., 2012. Lateral thigh fascia lata as interpositional graft for temporomandibular joint ankylosis. J Maxillofac Oral Surg 11, 354–357. https://doi.org/10.1007/s12663-011-0304-z

Bock, M.E., Nagle, R., Soyster, M., Song, L., Tachibana, I., Hathaway, J.K., Powell, C.R., 2021. Robotic Sacral Colpopexy Using Autologous Fascia Lata Compared with Mesh. Journal of Endourology 35, 801–807. https://doi.org/10.1089/end.2020.0537

Buergin, J., Werth, L., Largo, R., Scherberich, A., Schaefer, D.J., Kaempfen, A., 2022. Cross-sectional Vascularization Pattern of the Adipofascial Anterolateral Thigh Flap for Application in Tissue-engineered Bone Grafts. Plast Reconstr Surg Glob Open 10, e4136. https://doi.org/10.1097/GOX.0000000000004136

Dappa, E., Higashigaito, K., Fornaro, J., Leschka, S., Wildermuth, S., Alkadhi, H., 2016. Cinematic rendering – an alternative to volume rendering for 3D computed tomography imaging. Insights Imaging 7, 849–856. https://doi.org/10.1007/s13244-016-0518-1

de Spiegeleire, X., Vanhaebost, J., Coche, E., 2019. Post-mortem CT angiography of mesenteric vessels using cinematic rendering vision. Diagnostic and Interventional Imaging 100, 533–534. https://doi.org/10.1016/j.diii.2019.05.005

Disa, J.J., Goldberg, N.H., Carlton, J.M., Robertson, B.C., Slezak, S., 1998. Restoring abdominal wall integrity in contaminated tissue-deficient wounds using autologous fascia grafts. Plast Reconstr Surg 101, 979–986. https://doi.org/10.1097/00006534-199804040-00014

Ehrl, D., Heidekrueger, P.I., Schmitt, A., Liska, F., Ninkovic, M., Giunta, R., Broer, P.N., 2019. The Anterolateral Thigh Flap for Achilles Tendon Reconstruction: Functional Outcomes. Plast Reconstr Surg 143, 1772–1783. https://doi.org/10.1097/PRS.0000000000005652

Fawzi-Grancher, S., Goebbels, R.M., Bigare, E., Cornu, O., Gianello, P., Delloye, C., Dufrane, D., 2009. Human tissue allograft processing: impact on in vitro and in vivo biocompatibility. J Mater Sci Mater Med 20, 1709–20. https://doi.org/10.1007/s10856-009-3726-0

Ferretti, A., Monaco, E., Fabbri, M., Mazza, D., De Carli, A., 2017. The Fascia Lata Anterolateral Tenodesis Technique. Arthroscopy Techniques 6, e81–e86. https://doi.org/10.1016/j.eats.2016.09.005

Finn, M.A., Faulkner, N.D., Hetzel, S.J., Anderson, P.A., 2011. Spinal duraplasty materials and hydrostasis: a biomechanical study: Laboratory investigation. SPI 15, 422–427. https://doi.org/10.3171/2011.5.SPINE10851

Fox, P., Endress, R., Sen, S., Chang, J., 2014. Fascia-only anterolateral thigh flap for extremity reconstruction. Ann Plast Surg 72 Suppl 1, S9-13. https://doi.org/10.1097/SAP.0000000000000146

Imaizumi, A., Toyota, Y., 2022. One-stage reconstruction of the complex defects of the Achilles tendon and the adjoining calcaneus using the chimeric superolateral thigh flap: A case report. Microsurgery 42, 611–616. https://doi.org/10.1002/micr.30937

Janik, S., Hirtler, L., Traxler, H., Weninger, W.J., Seemann, R., Erovic, B.M., 2020. The vascularized fascia lata free flap: an anatomical study and clinical considerations. Eur Arch Otorhinolaryngol 277, 1733–1739. https://doi.org/10.1007/s00405-020-05861-8

Karaaltin, M.V., Batioglu-Karaaltin, A., Orhan, K.S., Demirel, T., Guldiken, Y., 2012. Autologous fascia lata graft for contour restoration and camouflage in tertiary rhinoplasty. J Craniofac Surg 23, 719–723. https://doi.org/10.1097/SCS.0b013e31824dbb92

Kimata, Y., Uchiyama, K., Ebihara, S., Nakatsuka, T., Harii, K., 1998. Anatomic variations and technical problems of the anterolateral thigh flap: a report of 74 cases. Plast Reconstr Surg 102, 1517–1523. https://doi.org/10.1097/00006534-199810000-00026

Koshima, I., Fukuda, H., Utunomiya, R., Soeda, S., 1989. The anterolateral thigh flap; variations in its vascular pedicle. Br J Plast Surg 42, 260–262. https://doi.org/10.1016/0007-1226(89)90142-2

Kuo, Y.-R., An, P.-C., Kuo, M.-H., Kueh, N.-S., Yao, S.-F., Jeng, S.-F., 2008. Reconstruction of knee joint soft tissue and patellar tendon defects using a composite anterolateral thigh flap with vascularized fascia lata. J Plast Reconstr Aesthet Surg 61, 195–199. https://doi.org/10.1016/j.bjps.2006.06.012

Lakhiani, C., Lee, M.R., Saint-Cyr, M., 2012. Vascular anatomy of the anterolateral thigh flap: a systematic review. Plast Reconstr Surg 130, 1254–1268. https://doi.org/10.1097/PRS.0b013e31826d1662

Lee, Y.-C., Chen, W.-C., Chou, T.-M., Shieh, S.-J., 2015. Anatomical Variability of the Anterolateral Thigh Flap Perforators: Vascular Anatomy and Its Clinical Implications. Plastic and Reconstructive Surgery 135, 1097–1107. https://doi.org/10.1097/PRS.0000000000001103

Leyssens, L., Pestiaux, C., Kerckhofs, G., 2021. A Review of Ex Vivo X-ray Microfocus Computed Tomography-Based Characterization of the Cardiovascular System. Int J Mol Sci 22, 3263. https://doi.org/10.3390/ijms22063263

Liang Yii, R.S., Chai, S.C., Zainal, H.M., Basiron, N., 2022. Single-stage reconstruction of a traumatic tendocutaneous defect of the Achilles using free composite anterolateral thigh flap with vascularized fascia lata. Jt Dis Relat Surg 33, 673–679. https://doi.org/10.52312/jdrs.2022.843

Lin, S.J., Rabie, A., Yu, P., 2010. Designing the anterolateral thigh flap without preoperative Doppler or imaging. J Reconstr Microsurg 26, 67–72. https://doi.org/10.1055/s-0029-1234023

Maes, A., Pestiaux, C., Marino, A., Balcaen, T., Leyssens, L., Vangrunderbeeck, S., Pyka, G., De Borggraeve, W.M., Bertrand, L., Beauloye, C., Horman, S., Wevers, M., Kerckhofs, G., 2022. Cryogenic contrast-enhanced microCT enables nondestructive 3D quantitative histopathology of soft biological tissues. Nat Commun 13, 6207. https://doi.org/10.1038/s41467-022-34048-4

Manon, J., Evrard, R., Fievé, L., Bouzin, C., Magnin, D., Xhema, D., Darius, T., Bonaccorsi-Riani, E., Gianello, P., Docquier, P.-L., Schubert, T., Lengelé, B., Behets, C., Cornu, O., 2023. A New Osteogenic Membrane to Enhance Bone Healing: At the Crossroads between the Periosteum, the Induced Membrane, and the Diamond Concept. Bioengineering 10, 143. https://doi.org/10.3390/bioengineering10020143

Manon, J., Evrard, R., Maistriaux, L., Fievé, L., Heller, U., Magnin, D., Boisson, J., Kadlub, N., Schubert, T., Lengelé, B., Behets, C., Cornu, O., 2022. Periosteum and fascia lata: Are they so different? Front. Bioeng. Biotechnol. 10, 944828. https://doi.org/10.3389/fbioe.2022.944828

Manon, J., Evrard, R., Maistriaux, L., Fieve, L., Xhema, D., Heller, U., Broeck, L.VAN.DEN., Vettese, J., Boisson, J., Schubert, T., Lengele, B., Behets, C., Cornu, O., 2024a. HLA Awareness in Tissue Decellularization: A Paradigm Shift for Enhanced Biocompatibility, studied on the Model of the Human Fascia Lata Graft. Biomaterials 122741. https://doi.org/10.1016/j.biomaterials.2024.122741

Manon, J., Fodjeu, G., Evrard, R., den Broeck, L.V., Jacob, M., Coche, E., Cornu, O., Behets, C., Lengelé, B., 2024b. A single Angiofil-latex injection for both radiological and anatomical assessment of arterial territories in the limbs. Annals of Anatomy - Anatomischer Anzeiger 256, 152312. https://doi.org/10.1016/j.aanat.2024.152312

Manon, J., Gallant, L., Gérard, P., Fieve, L., Schneidewind, P., Pyka, G., Kerckhofs, G., Lengelé, B., Cornu, O., Behets, C., 2024c. 2D and 3D microstructural analysis of the iliotibial tract. Journal of Anatomy 00, 1–15. https://doi.org/10.1111/joa.14125

Matthewson, G., Coady, C.M., Wong, I.H.-B., 2020. Rotator Cuff Reconstruction Using Fascia Lata Patch Autograft for the Nonrepairable Rotator Cuff Tear. Arthroscopy Techniques 9, e123–e130. https://doi.org/10.1016/j.eats.2019.09.006

May, J.G., Kerr, J., May, J.A., Tassone, P., Rivera, A.L., 2022. The use of a simultaneous fascia lata-free flap with cochlear implantation after radical Mastoidectomy. Clinical Case Reports 10, e6159. https://doi.org/10.1002/ccr3.6159

Pirri, C., Petrelli, L., Fede, C., Guidolin, D., Tiengo, C., De Caro, R., Stecco, C., 2023. Blood supply to the superficial fascia of the abdomen: An anatomical study. Clinical Anatomy 36, 570–580. https://doi.org/10.1002/ca.23993

Saint-Cyr, M., Oni, G., Lee, M., Yi, C., Colohon, S.M., 2012. Simple Approach to Harvest of the Anterolateral Thigh Flap: Plastic and Reconstructive Surgery 129, 207–211. https://doi.org/10.1097/PRS.0b013e318233ef4a

Saint-Cyr, M., Schaverien, M., Arbique, G., Hatef, D., Brown, S.A., Rohrich, R.J., 2008. Three- and four-dimensional computed tomographic angiography and venography for the investigation of the vascular anatomy and perfusion of perforator flaps. Plast Reconstr Surg 121, 772–780. https://doi.org/10.1097/01.prs.0000299338.97612.90

Sananpanich, K., Tu, Y.K., Kraisarin, J., Chalidapong, P., 2008. Flow-through anterolateral thigh flap for simultaneous soft tissue and long vascular gap reconstruction in extremity injuries: anatomical study and case report. Injury 39 Suppl 4, 47–54. https://doi.org/10.1016/j.injury.2008.08.031

Sapino, G., Zaugg, P., Cherix, S., Borens, O., Lo, S.J., Raffoul, W., di Summa, P.G., 2019. ALT flap with vascularized fascia lata for one-stage functional patellar tendon reconstruction. Journal of Plastic, Reconstructive & Aesthetic Surgery 72, 467–476. https://doi.org/10.1016/j.bjps.2018.11.002

Shieh, S.J., Chiu, H.Y., Yu, J.C., Pan, S.C., Tsai, S.T., Shen, C.L., 2000. Free anterolateral thigh flap for reconstruction of head and neck defects following cancer ablation. Plast Reconstr Surg 105, 2349–2357; discussion 2358-2360. https://doi.org/10.1097/00006534-200006000-00006

Smith, R.K., Wykes, J., Martin, D.T., Niles, N., 2017. Perforator variability in the anterolateral thigh free flap: a systematic review. Surg Radiol Anat 39, 779–789. https://doi.org/10.1007/s00276-016-1802-y

Song, S.H., Choi, S., Kim, Y.-M., Lee, S.R., Choi, Y.W., Oh, S.-H., 2013. The composite anterolateral thigh flap for knee extensor and skin reconstruction. Arch Orthop Trauma Surg 133, 1517–1520. https://doi.org/10.1007/s00402-013-1833-3

Song, Y.G., Chen, G.Z., Song, Y.L., 1984. The free thigh flap: a new free flap concept based on the septocutaneous artery. Br J Plast Surg 37, 149–159. https://doi.org/10.1016/0007-1226(84)90002-x

Song, Z., Yang, D., Yang, J., Nie, X., Wu, J., Song, H., Gu, Y., 2018. Abdominal wall reconstruction following resection of large abdominal aggressive neoplasms using tensor fascia lata flap with or without mesh reinforcement. Hernia 22, 333–341. https://doi.org/10.1007/s10029-018-1738-8

Sreenath, S.B., Grafmiller, K.T., Tang, D.M., Roof, S.A., Woodard, T.D., Kshettry, V.R., Recinos, P.F., Sindwani, R., Fritz, M.A., 2023. Free Tissue Transfer for Skull Base Osteoradionecrosis: A Novel Approach in the Endoscopic Era. Laryngoscope 133, 562–568. https://doi.org/10.1002/lary.30315

Stecco, C., Tiengo, C., Stecco, A., Porzionato, A., Macchi, V., Stern, R., De Caro, R., 2013. Fascia redefined: anatomical features and technical relevance in fascial flap surgery. Surg Radiol Anat 35, 369–376. https://doi.org/10.1007/s00276-012-1058-0

Tokumoto, H., Akita, S., Mitsukawa, N., Hasegawa, M., Kubota, Y., Adachi, N., Suzuki, T., Satoh, K., 2016. An anatomical and histological study of the vascularized iliotibial tract graft. Microsurgery 36, 325–329. https://doi.org/10.1002/micr.30006

Tomaszewski, K.A., Vikse, J., Henry, B.M., Roy, J., Pękala, P.A., Svensen, M., Guay, D., Saganiak, K., Walocha, J.A., 2017. The variable origin of the lateral circumflex femoral artery: a meta-analysis and proposal for a new classification system. Folia Morphol (Warsz) 76, 157–167. https://doi.org/10.5603/FM.a2016.0056

van Steenberghe, M., Schubert, T., Guiot, Y., Bouzin, C., Bollen, X., Gianello, P., 2017. Enhanced vascular biocompatibility of decellularized xeno-/allogeneic matrices in a rodent model. Cell Tissue Bank 18, 249–262. https://doi.org/10.1007/s10561-017-9610-0

Vettese, J., Manon, J., Chretien, A., Evrard, R., Fievé, L., Schubert, T., Lengelé, B.G., Behets, C., Cornu, O., 2024. Collagen molecular organization preservation in human fascia lata and periosteum after tissue engineering. Front. Bioeng. Biotechnol. 12. https://doi.org/10.3389/fbioe.2024.1275709

Xu, D.C., Zhong, S.Z., Kong, J.M., Wang, G.Y., Liu, M.Z., Luo, L.S., Gao, J.H., 1988. Applied anatomy of the anterolateral femoral flap. Plast Reconstr Surg 82, 305–310.

Youn, S.K., Kim, S.W., Kim, Y.H., Hwang, K.T., 2015. The composite anterolateral thigh flap for achilles tendon and soft tissue defect reconstruction with tendon repair by fascia with double or triple folding technique. Microsurgery 35, 615–621. https://doi.org/10.1002/micr.22490

Yu, P., 2004. Characteristics of the anterolateral thigh flap in a Western population and its application in head and neck reconstruction. Head & Neck 26, 759–769. https://doi.org/10.1002/hed.20050

## Tables

*Table 1. Demographics of each part of the anatomical study.*

| | ***Number of limbs*** | ***Number of donors*** | ***Sex*** | ***Age*** *(mean ± SD)* | ***Laterality*** |
|---|---|---|---|---|---|
| *Distribution of the LCFA (CT + dissection)* | *11* | *8* | *6 ♂ / 2 ♀* | *80.1 ± 15.3* | *5 L / 6 R* |
| *Intrinsic vascularization of the FL (Dissection + microCT)* | *5* | *5* | *3 ♂ / 2 ♀* | *84.7 ± 6.1* | *0 L / 5 R* |
| *Total* | 16 | 13 | 9 ♂ / 4 ♀ | 81.9 ± 12.4 | 5 L / 11 R |

*SD: standard deviation, LCFA: lateral circumflex femoral artery, CT: computed tomography, FL: fascia lata, microCT: microfocus X-ray computed tomography, ♂: men, ♀: women, L: left, R: right.*

*Table 2. MicroCT acquisition and image processing parameters*

| **Acquisition parameters** *Low-resolution* | | **Acquisition parameters** *High-resolution* | |
|---|---|---|---|
| *Voxel size (µm)* | 66.6 | *Voxel size (µm)* | 15 |
| *Source voltage (kV)* | 65 | *Source voltage (kV)* | 65 |
| *Tube current (µA)* | 350 | *Tube current (µA)* | 400 |
| *Exposure time (ms)* | 500 | *Exposure time (ms)* | 500 |

| *Number of images* | 2800 | *Number of images* | 3200 |
|---|---|---|---|
| *Average** | 1 | *Average** | 1 |
| *Skip** | 0 | *Skip** | 0 |
| *Acquisition time (min)* | 23 | *Acquisition time (min)* | 26 |

**Information about those parameters was previously given in the literature* (Maes et al., 2022)

*Table 3. Distribution and pattern of perforators according to Yu's ABC classification (Yu, 2004) after dissection.*

| ***Yu's ABC classification*** | ***Perforators*** *n (%)* | ***Septocutaneous*** *n (%)* | ***Musculocutaneous*** *n (%)* | ***Limb with one perforator*** *n (%)* |
|---|---|---|---|---|
| *A* | *9 (32.1%)* | *6 (66.7%)* | *3 (33.3%)* | *9 (81.8%)* |
| *B* | *10 (35.7%)* | *6 (60.0%)* | *4 (40.0%)* | *11 (100%)* |
| *C* | *9 (32.1%)* | *0 (0.0%)* | *9 (100%)* | *9 (81.8%)* |
| *Total* | 28 (100%) | 12 (43%) | 16 (57%) | 11 (100%) |

*n: number, %: percentage. The percentage of perforators was calculated on the total number of perforators (n=28). The percentages of septo- and musculocutaneous perforators were calculated on the number of perforators of the respective level ABC. The percentage of limbs with one perforator was calculated on the total number of limbs (N=11).*

## Figure legends

*Figure 1. Study design of the experiment. Harvesting of the full-thickness fasciocutaneous anterolateral thigh flap (N=5 donors), seen from its deep surface and divided into two parts, the fascia lata (FL) and the iliotibial tract (ITT) (a). Cubes of 2x2cm are harvested, centered on the perforating artery (P2 for example in this figure) (n=3 cubes x 3 donors=9) (b). Full-thickness cubes were imaged with microCT and extraction of subvolume containing only the FL tissue was highlighted in light blue (c), which directly permitted the quantification of the vasculature volume inside the FL (d). Autoskeleton module allowed to skeletonize the vascular network into segments and branching nodes that were quantified. Dark blue arrows: Orientation thread in the antero-superior corner. Note that the harvested samples are somewhat distorted by the fixation threads sutured at the four corners of the cube, which thus takes the form of a cushion. This artifact slightly alters the native parallelism between the anatomical planes of the deep fascia and skin surface, as well as the native disposition of vascular networks. White scale bar: 5mm.*

*Figure 2. Macroscopic visualization of perforating arterioles: ramified perforator in the subfascial gliding plane (a), isolated perforator (b), and perforating vessel that branches in/after the fascia lata (FL) (c). DF: deep fat, SF: superficial fat. Yellow arrowheads show ramified branches, running along the FL. Red arrowhead marks the continuity of the main perforating arteriole. The thin dotted line runs along the superficial fascia.*

*Figure 3. Low-resolution Angiofil-latex enhanced microCT of the whole ALT flap divided into two parts, the fascia lata (FL) and the iliotibial tract (ITT) (a). High-resolution Angiofil-latex*

*enhanced microCT cross-section of a full-thickness cube (b) and 3D renderings (c) highlighting the extrinsic vascularization (red) and the intrinsic vascularization (yellow), emerging from a perforating arteriole (P), before and after removing the segmented FL in grey. DF: deep fat, SF: superficial fat. White arrowheads: intrinsic vessels. White scale bars: 5mm, pink scale bar: 1mm.*

## Appendices

*Additional Table A. Vascular patterns present in this study after dissection (N=11), out of the 19 patterns described by the combination of Yu's ABC system and Shieh's vascular classification(Lee et al., 2015; Yu, 2004). Yu's classification identifies three levels or perforator localization, i.e. at the midpoint between the anterior superior iliac spine and the patella (perforator B), and 5cm proximally (perforator A) or distally (perforator C) from this point. Shieh's classification focused on the perforator origin, number, and location.*

| | | Double perforators | | Triple perforators | |
|---|---|---|---|---|---|
| **Pedicle origin** | **A+B** | **B+C** | **A+C** | **A+B+C** | ***Total*** |
| **DB** | **9% (n=1)** 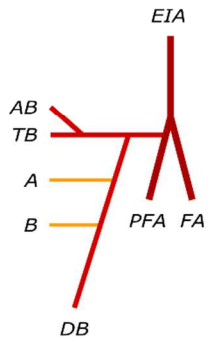  | **9% (n=1)** 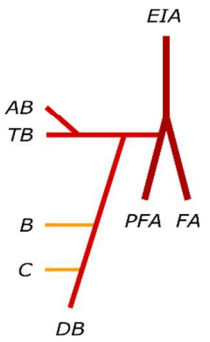  | **0% (n=0)** 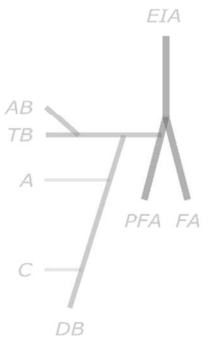  | **0% (n=0)** 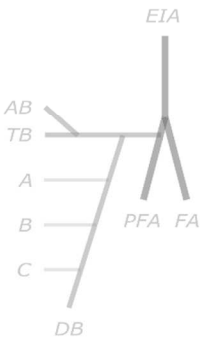  | **18%** |
| **TB** | **9% (n=1)** 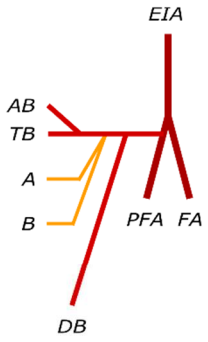  | **0% (n=0)** 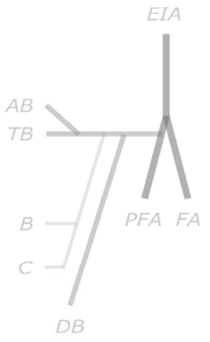  | **0% (n=0)** 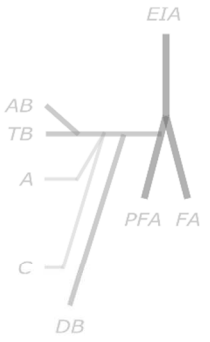  | **0% (n=0)** 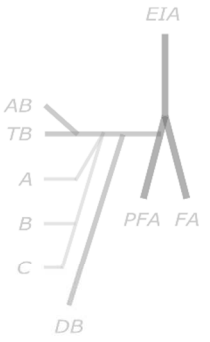  | **9%** |
| **DB+TB** | **0% (n=0)** 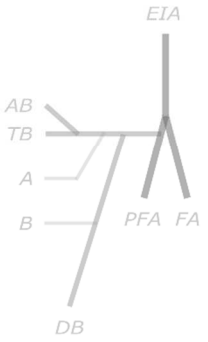  | **9% (n=1)** 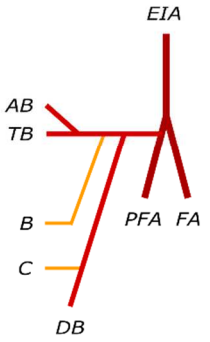  | **9% (n=1)** 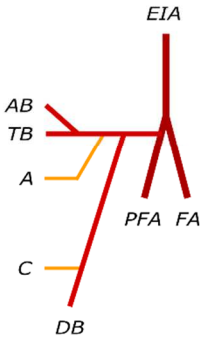  | **55% (n=6)** 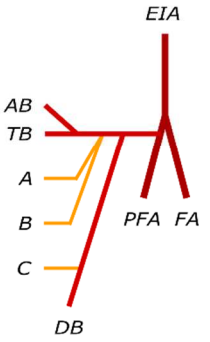  | **73%** |
| ***Total*** | **18%** | **18%** | **9%** | **55%** | **100%** |

*DB: descending branch, TB: transversal branch, AB: ascending branch, FA: femoral artery, EIA: external iliac artery, PFA: profunda femoris artery, FA: femoral artery, n: number.*

# Beneath the Perforators: Unravelling Fascia Lata Intrinsic Vascular Architecture

Macroscopic analysis (Dissection)

Microscopic analysis (MicroCT imaging)